

First principles approaches and concepts for electrochemical systems

Mira Todorova^{1*}, Stefan Wippermann^{1,2*} and Jörg Neugebauer^{1*}

^{1*}Max-Planck-Institut für Eisenforschung, Max-Planck-Str. 1, Düsseldorf, 40237, Germany.

^{2*}Philipps-Universität Marburg, Renthof 5, Marburg, 35032, Germany.

*Corresponding author(s). E-mail(s): m.todorova@mpie.de; s.wippermann@mpie.de; j.neugebauer@mpie.de;

Ab initio techniques have revolutionized the way how theory can help practitioners to explore critical mechanisms and devise new strategies in discovering and designing materials. Yet, their application to electrochemical systems is still limited. A well known example how novel concepts can boost our ability to perform such studies is the introduction of temperature control into *ab initio* simulations. The analogous technique to model electrochemical systems – potential control – is just emerging.

In this review, we critically discuss state-of-the-art approaches to describe electrified interfaces between a solid electrode and a liquid electrolyte in realistic environments. By exchanging energy, electronic charge and ions with their environment, electrochemical interfaces are thermodynamically open systems. In addition, on the time and length scales relevant for chemical reactions, large fluctuations of the electrostatic potential and field occur. We systematically discuss the key challenges in including these features in realistic *ab initio* simulations, as well as the available techniques and approaches to overcome them, in order to facilitate the development and use of these novel techniques to the wider community. These methodological developments provide researchers with a new level of realism to explore fundamental electrochemical mechanisms and reactions from first principles.

1 Transferring the macroscopic electrochemical cell into a DFT supercell

Achieving an atomic scale understanding of electrochemical processes is imperative to achieve breakthrough innovations. Examples are new generations of supercapacitors [1–5], metal-air-batteries [6–10], transient electronics [11–14], or new concepts in sustainable metallurgy [15–18]. First principles electronic structure techniques are the method of choice. While these techniques are routinely employed in many fields, their application to electrochemical systems is still limited.

A key challenge in describing electrochemical systems and reactions by *ab initio* techniques is the large range of relevant length and time scales [19]. The three relevant scales are schematically sketched in Fig. 1. The actual technical system typically of interest is a full cell consisting of two charged electrodes connected to a potentiostat and immersed in an electrolyte (macroscopic scale). A characteristic feature of electrochemical systems is that the applied voltage in the macroscopic system does not drop homogeneously but only in a small region near the electrode-interface. Away from the electrodes the potential is constant, i.e., the system in this region is field free and charge neutral and is, unlike a capacitor, not affected by the electrode distance. From a modeling perspective it can thus easily be captured by suitable boundary conditions.

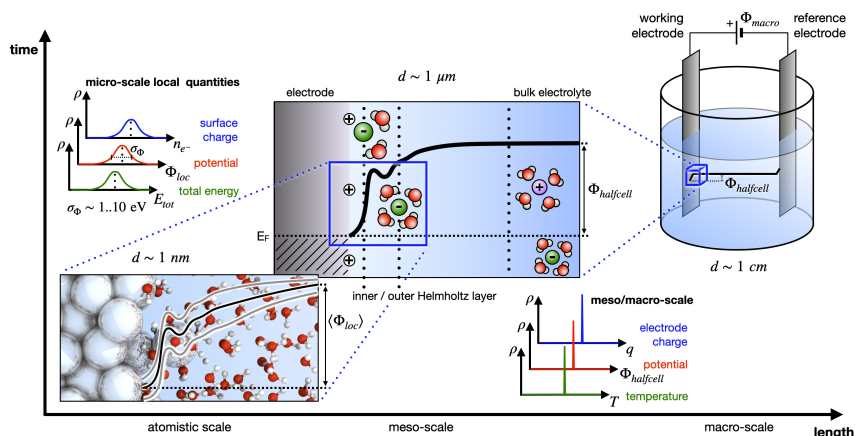


Fig. 1 Schematic representation of an electrochemical system at the three major length- and time-scales - macroscopic, mesoscopic and microscopic - together with the respective electrostatic potential perpendicular to the solid/liquid interface. The distribution of key electrochemical quantities such as surface charge, potential and total energy are shown for the microscopic (top-left) and the meso/macro-scale (bottom-right).

The induced potential is localized in a small region near the electrode-electrolyte interface, resulting in rapid changes in the electrostatic potential close to the electrode (mesoscopic scale). The largest drop and thus the highest electric fields are within the inner and outer Helmholtz layers, which extend

over a range of about 1 nm. This length scale corresponds to the atomistic scale and can be represented by modern DFT supercell calculations. While the electrochemically and electrocatalytically most relevant region with the largest electric fields fits within the supercell, many of the control-parameters and boundary conditions, such as the local potential, the surface charge or the total energy, are not constant but show large variations. These are schematically sketched as inset in Fig. 1 by their corresponding density of states, each of which exhibits due to its thermal origin a normal (Gaussian) distribution. It is important to note that this is solely related to the small size of conventional DFT supercells. On the meso- or macroscale, these quantities result from averaging over large areas, essentially yielding constant (delta-function like distributions) as shown in the bottom right inset. Conceptually, these averaged macroscopic quantities can be obtained by performing thermodynamically open supercell calculations (to achieve the desired fluctuations) and average over the resulting supercell configurations.

This concept of stochastic sampling of physical quantities in the supercell is common when performing molecular dynamics (MD) simulations at constant temperature [20–25]. The correct magnitude of fluctuations in the total energy of the supercell is achieved by applying a thermostat. The thermostat resembles an infinite reservoir with which the supercell exchanges energy to keep the average temperature in the supercell at a predefined value. For finite temperature MD simulations the application of thermostats controls both the average temperature and the thermodynamically consistent distribution of energy fluctuations. The fundamental relation between energy dissipation (to control the temperature) and fluctuations (the stochastic noise term describing the energy fluctuations) is given by the dissipation-fluctuation theorem [26].

While temperature control with thermostats is common and a well-established practice for MD simulations, the application of potentiostats in *ab initio* MD (AIMD) simulations is still rare [19]. The reason is on one side the difficulty in setting up computational electrodes. On the other side, most computational setups assume constant voltage or constant charge conditions. While these are the appropriate boundary conditions for the mesoscopic/-macroscopic case, as shown in Fig. 1, they fail to capture the voltage and charge fluctuations present on the atomistic level.

In this review, we therefore discuss first in Sec. 2 the various electrostatic boundary conditions and their potential shortcomings when applied within a periodic supercell approach. Sec. 3 reviews available designs of computational electrodes, which are used to induce a potential drop across the electrochemical interface between the working electrode and the electrolyte. Sec. 4 focuses on challenges in applying electric fields in the context of electronic structure simulations, such as band alignment or dielectric breakthrough. Sec. 5 discusses how to set-up *ab initio* calculations with open thermodynamic boundary conditions, which account for the exchange of electrons with an external reservoir and enable potential control. Finally, we point in the conclusions to some of the challenges in modelling electrified solid/liquid interfaces, which remain open.

4 *First principles approaches and concepts for electrochemical systems*

Multiple further topics related to *ab initio* simulations of electrochemical solid/liquid interfaces may be of interest, but are not covered in this review. We therefore encourage interested readers to look into the following reviews about implicit solvents [27], the electric double-layer [28], the use of phase diagrams in modelling corrosion [29], electrocatalysis [30, 31], electrochemical energy conversion and storage [32], energy materials applications [33] or water at charged interfaces [34].

2 Electrostatic boundary conditions

Fig. 2 provides a schematic overview about the three main cases to setup electrostatic boundary conditions. To understand the impact of the specific boundary condition we consider its ability to correctly describe a key feature of an electrostatic interface namely the energetics and reaction rates of electrochemical interactions. As prototype example we consider here the case of an initially neutral atom or molecule at the interface (marked as initial in Fig. 2) that is positively charged (marked as final) after the reaction. Examples for this type of electrochemical reaction can be the dissolution of a metal surface in contact with water (wet corrosion) [35–37] or a reaction step in an electro-catalytic reaction [38–41]. The driving forces for this reaction are on one side the large solvation energy an atom or molecule can gain when becoming charged and/or the presence of the strong electric fields at such interfaces which energetically favor the movement of charge along the field.

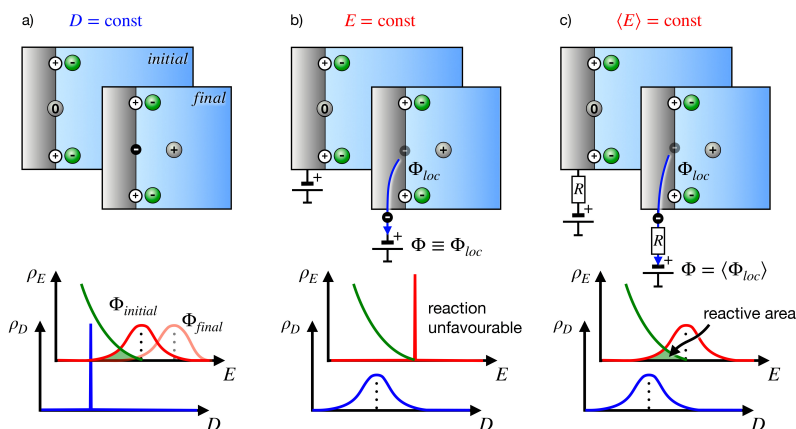


Fig. 2 Schematic representation of the possible electrostatic boundary conditions, as well as their associated electric (ρ_E) and displacement (ρ_D) field distributions. The circles with positive (+) and negative (-) charges depict a prototypical reaction. The green shaded area in the electric field distribution plot shows the region within which the reaction can occur.

A product of the here considered prototype reaction, namely a single atom which is (singly) positively charged after the reaction, is an extra electron,

which initially will stay on the surface. A key question when modeling such a reaction is what happens to this extra charge on the surface and are the boundary conditions adequate to reproduce the behaviour of the macroscopic system?

As a first scenario we consider constant charge conditions. In this case, the net charge on the electrode where the reaction takes place and on the counter electrode (not shown here) is kept fixed and its sum is zero, i.e., the total setup of electrode and counter electrode is charge neutral. This scenario corresponds to constant electric displacement D and is sketched in Fig. 2a. At constant charge conditions the number of excess charges (shown as white circles with a plus at the electrode) is fixed. Consequently, the extra electron created by the charge transfer reaction cannot be compensated and forms together with the positive ion an electric dipole along the surface normal. For a supercell geometry with periodic boundary conditions, this dipole is infinitely repeated laterally giving rise to an effective capacitance and thus a large surface dipole. As a consequence, the average potential $\langle \Phi \rangle$ will be significantly shifted away from the initial voltage.

Thus, whenever performing simulations where the interface dipole may change, e.g., due to electrochemical reactions, changes in the surface or adsorbate geometry etc., these boundary conditions are unable to reproduce constant voltage conditions. For characteristic supercell sizes used for modelling the electrochemical interface the average voltage can easily shift by an amount on the order of ~ 1 eV [38, 42, 43]. Constant charge boundary conditions are therefore also not well-suited to accurately describe reaction rates, since the barrier for an electrochemical reaction scales with the electric field like $\mathcal{E}_{\text{barrier}}(E) = \mathcal{E}_{\text{barrier}}^0 - [\int E(\vec{r}') d\vec{r}'] \cdot q$, where $\mathcal{E}_{\text{barrier}}^0$ is the zero-field barrier, $E(\vec{r}, t)$ the local electric field and q the charge transferred in the reaction. The reaction rate is the convolution of the barrier and the Boltzmann distribution, $w_{\text{reaction}} \propto \int_{-\infty}^{\infty} \rho_{\mathcal{E}}(E) \cdot e^{-\mathcal{E}_{\text{barrier}}(E)/k_{\text{B}}T} dE$, with temperature T , Boltzmann constant k_{B} and field distribution $\rho_{\mathcal{E}}(E)$. The integral over E where reactions can take place is marked by the green area (labelled reactive area) in the field distribution plots in Fig. 2. As shown there, the reactive area before and after the reaction changes dramatically, making constant charge boundary conditions also unsuitable for describing reactions.

We note, however, that for computing equilibrium quantities - such as the potential of zero charge (PZC) - for a surface in contact with an electrolyte, the constant charge approach ($D = \text{const}$) for the special condition of zero charge is well suited and has been successfully employed in several studies [44, 45]. The reason why these boundary conditions work well in this case is that in the absence of chemical reactions the surface structure remains unchanged and the PZC is characterized by the condition that no net charge is transferred to or away from the electrode, which is automatically given by the condition $q = \text{const}$.

The second scenario assumes that the voltage Φ is kept constant, i.e., fluctuations in the potential are not possible ($\Phi \equiv \langle \Phi \rangle$), see density distribution

for E in Fig. 2b. To keep the potential constant, charges can be exchanged (i.e. flow back and forward) with the potentiostat. Thus, for the model reaction considered here, once the extra electron is at the electrode a charge q will be transferred until the shift between initial and final potential becomes zero. Therefore, these boundary conditions provide a realistic description of the electrochemical current that flows when keeping the voltage constant and charge transfer reactions take place. Experimentally, this would be measured as current-voltage (U-I) characteristic. While the resulting net current can be described, the lack of the thermally induced fluctuations in the electric field implies a qualitatively different reactive area. As an analogy, in the theory of thermostats it is well understood that “[...] for small systems or when the observables of interest are dependent on the fluctuations rather than on the averages [...]” [46], such a method cannot be used. For polar systems such as water, thermal fluctuations cause fluctuations in the net interface dipole, which lead to fluctuations in the potential Φ . Since these voltage fluctuations represent the actual physics of the system, it is important to not constrain them artificially by the condition of constant voltage (cf. density distribution of E in Fig. 2b). Due to the absence of fluctuations, electric fields that are more beneficial for the reaction are absent.

Since the voltage distribution for typical DFT supercell sizes is in the order of a few eV, whereas the characteristic thermal energy at room temperature $k_B T$ is only 25 meV, Boltzmann population will occupy mainly the energetically low-lying states, which are missing at constant voltage (cf. Fig. 2b).

The most general boundary conditions for the supercell are the thermodynamically open ones, both with respect to charge transfer and fluctuations, as well as to voltage control (e.g. $\langle \Phi \rangle = \text{const.}$), cf. Fig. 2c. These boundary conditions are able to describe the electrochemical net current in analogy to the constant voltage approach, but without any artificial constraints on either the field or the charge fluctuations. Unlike the $D = \text{const}$ and $E = \text{const}$ approaches, where the reactive area is either changing or entirely missing, these open boundary conditions preserve the reactive area before and after the reaction (see distributions in Fig. 2c).

Fully open boundary conditions imply, however, that the system is able to perform external work $\Delta W = \Delta q \cdot \Delta E$, where Δq and ΔE are the change in the charge and the electric field, respectively. In the first two scenarios (cf. distributions in Figs. 2a,b) either Δq or ΔE is artificially enforced to be exactly zero, so that $\Delta W \equiv 0$. Under open boundary conditions, however, ΔW becomes finite. The finite ΔW permits the system on short time scales to “borrow” energy from the ensuing charge and potential fluctuations, in analogy to the theory of thermostats [46]. This ability to perform external work is necessary in order to preserve the reactive area before and after the reaction, as illustrated in Fig. 2c. On the other hand, the finite ΔW implies that introducing potential control via relaxing $\Phi(t)$ towards its targeted mean $\langle \Phi \rangle$ dissipates energy (represented schematically by the resistor in Fig. 2c).

In order to balance the energy dissipated due to potential control, one may be tempted to replenish the dissipated energy via an explicit thermostat. We emphasize, however, that a thermostat acts indiscriminately on all degrees of freedom, whereas a potentiostat is able to affect only those vibrational degrees of freedom that couple to a change in the ensemble's dipole moment parallel to the direction of the applied electric field. Draining energy from one set of degrees of freedom and subsequently returning it to another invariably leads to a spurious energy transfer between them. Such an approach cannot restore the system to equilibrium. On the contrary, it would constantly drive the system out of equilibrium [47].

Thus, any open boundary potential control scheme must therefore simultaneously introduce a thermodynamically consistent distribution of charge and potential fluctuations. The fundamental relation between energy dissipation (to control, e. g., the temperature, pressure or potential) and fluctuations (to balance the dissipation in thermodynamic equilibrium) is provided by the fluctuation-dissipation theorem (FDT) [26]. Analogous to thermostats, where an equation of motion for the exchange of heat with an external bath is derived from the FDT and that are nowadays widely used in MD simulations, constructing a potentiostat involves deriving an equation of motion for the exchange of charge with an external voltage source [48] via the FDT [49].

These fully open boundary conditions [48, 49] accurately reproduce in a supercell sized box the behavior of voltage and charge measured within the full macroscopic system. These conditions are thus able to describe all aspects of an electrochemical system including electrochemical reactions or dynamic changes in the surface or adatom structure. Only when computing the intrinsic electrode potential of a system, constant (zero) charge boundary conditions may be used.

3 Design of a computational counter electrode

Realizing potential control - as outlined above - in electronic structure simulations, requires the ability to apply an electric field or introduce a charge on the electrode surface, so that the field distribution inside the supercell accurately describes the real physical system (cf. atomistic scale in Fig. 1). To avoid a singularity in the electrostatic energy when using supercells with periodic boundary conditions the cell must be charge neutral. As a consequence, the excess charge at the surface must be exactly compensated by an opposite charge. If no explicit compensating charge is added, DFT codes drop the $G = 0$ plane wave component in Fourier space, resulting effectively in a spatially homogeneous background charge which exactly compensates for the excess charge at the surface.

To provide more control in achieving realistic field distributions, a computational counter electrode is included. We emphasize that the computational counter electrode does not play the role of any physical electrode (i.e. neither the physical counter electrode nor the reference electrode). Its sole purpose is

to compensate for the charge at the electrified surface, to introduce the desired field distribution in the microscopic region targeted by the simulations, and to provide the boundary conditions set by the electrochemical environment that is external to the simulation cell. In other words, the computational counter electrode accounts for the residual charge of that part of the electric double layer, that is located outside the simulation cell. Therefore, inside the simulation cell, the field and potential distributions of the simulated system are equal to the ones of the macroscopic physical system within the electrochemically active region. Outside the simulation cell, the potentials differ by an offset, cf. Fig. 3. Suitable corrections can be straightforwardly derived and applied *a posteriori* via purely electrostatic modelling without the need for simulations at the electronic structure level of theory.

Realizing a suitable computational counter electrode is a challenging task. Most density-functional theory (DFT) simulations for electrode-electrolyte interfaces are performed using supercell calculations in periodic boundary conditions (PBCs) [50–56]. The use of PBCs, which is required in order to describe extended interfaces, strictly enforces (i) simulation cells that are charge neutral in total (due to Gauss’s law in electrostatics) and (ii) electric field distributions that obey the periodicity of the supercell. Moreover, (iii) in available DFT codes there is only a single Fermi level that is constant throughout the supercell. It is thus explicitly impossible to maintain a working electrode and a counter electrode within the same supercell at different Fermi levels in standard DFT simulations.

Therefore, while it is trivial in the case of thermostats or barostats to adjust the control parameter (i.e. the kinetic energy or the cell volume, respectively), this is considerably more difficult in the case of potentiostats (electrode

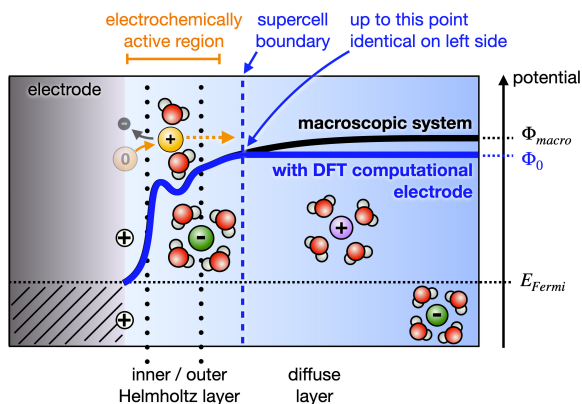


Fig. 3 Comparison between the potential in the macroscopic system and the potential obtained in DFT supercell simulations via a computational electrode. The potentials agree within the microscopic electrochemically active region. The fraction of the double layer charge that is located beyond the boundaries of the supercell must be placed on the DFT computational electrode to ensure charge neutrality. Therefore, at larger distances both potentials differ by a constant amount. A suitable correction can be performed *a posteriori*.

charge). Multiple approaches to apply fields or charges in supercells have thus been explored over the past decades, to address the restrictions outlined above. Fig. 4 provides a schematic overview of the main computational setups.

One of the earliest approaches was suggested by Neugebauer and Scheffler [57], extending the dipole correction [58] to place a slab in a capacitance. Later, Lozovoi and Alavi [59] used a symmetric slab setup, cf. Fig. 4a, where the surfaces are charged by introducing a net charge to the system. In order to ensure charge neutrality of the super cell, an equal and opposite homogeneous background charge is used as a computational counter electrode. While this setup can be easily applied in any DFT code, it is unable to provide a direct measure for the electrode potential: in principle, the electrode potential is given by the derivative $\Phi = \frac{\partial \mathcal{H}}{\partial q}$ of the DFT total energy \mathcal{H} with respect to the charge q , which is, however, a notoriously difficult quantity to compute in 3D PBC supercell calculations [60, 61]. Also, the distribution of the counter-charge as homogeneous background is very different from the distribution of the counter-charges in a realistic electrochemical cell. In the latter, the counter-charges are realized by the counter-electrode and the net-charge of the solvated ions in the electrolyte, which show a distribution very different from a spatially homogeneous and constant background.

Otani *et al.* therefore proposed to use 2D PBCs to describe the lateral periodicity of the interface, while lifting the PBC parallel to the surface normal via Green's function techniques [62–64], cf. Fig. 4b. Alternatively, one may lift the PBCs selectively only for the electric field in the supercell via electric enthalpy-based approaches [65] or Berry phase techniques [66] and the modern theory of polarization [67, 68], cf. Fig. 4c. Here, the electrostatic potential drop across the supercell is described by a geometric phase, which accumulates when moving from one periodic image of the supercell to the next. Such approaches to describe electric fields in supercells are demanding to implement. Hence, they are available in only some of the $\sim 40+$ publicly available DFT codes [69]. Moreover, the practical implementations of this approach work typically only for systems with a bandgap. Thus, only systems containing semiconductor or insulator electrodes can be studied.

For this reason, minimally invasive approaches working within the constraints of 3D PBC have been exploited, as well. Multiple groups proposed [70–73] to vary the number of H^+ ions contained within the DFT supercell grand-canonically. For the same purpose, Cucinotta *et al.* [74] introduced an intentionally unbalanced number of cations and anions in the electrolyte. Both approaches give rise to an uncompensated net-charge. Since the total system is charge neutral, the non-compensated charge accumulates at the interface, cf. Fig. 4d. By construction, this charge can assume only integer values. Even when using rather large supercells, the number of possible charge states at the interface is rather limited. This limited number of charge states at the interface severely restricts the variability of the ensuing electric fields and, hence, the applicability of techniques to sample thermodynamically open boundary conditions with $\langle \Phi \rangle = \text{const.}$

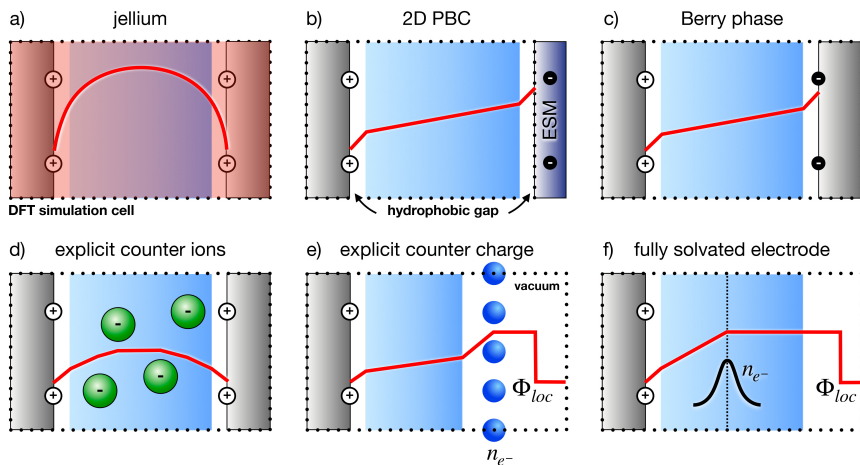


Fig. 4 The various approaches used to achieve a charged (electrified) electrode-electrolyte interface within a DFT supercell. Electrodes are shown as grey rectangles at the edge(s) of the supercell (marked by a dotted line) and the electrolyte as a blue area within it. The red hue covering the supercell in a) represents the homogeneous background charge. Ions and charges at the electrodes are shown as spheres containing a plus or minus, while atoms are shown as coloured spheres. The resulting electrostatic potential curve is depicted by the red line.

A continuous variation of the charge on the working electrode is achieved via charged implicit solvents [75, 76]. Also, hybrid solvation schemes have been suggested, where a region of explicit electrolyte is complemented by a charged implicit solvent or continuum dielectric [77, 78], which are placed at the edge of the explicit electrolyte region. Hybrid approaches of this type require an implementation within the respective electronic structure package. For this reason, Surendralal *et al.* [79] proposed to replace the charged implicit region by an explicit atomistic counter electrode. This approach uses pseudo-atoms, i.e. neutral objects with fractional proton numbers [80], to charge the working electrode. The employed setup introduces an explicit counter electrode consisting of Ne pseudo-atoms and a vacuum region into the supercell, and is shown in Fig. 4e. Apart from enabling a continuous variation of the charge within the supercell, this approach has also the advantage, that: (i) it avoids the use of a compensating background, since the overall supercell remains neutral, (ii) all its design elements can be easily realized in a standard DFT code and do not require changes to the code and (iii) it works equally well with metallic and semiconducting electrodes. Moreover, Surendralal *et al.*'s setup is straightforwardly extended to describe fully open boundary conditions for the electrode charge [47]. Dudzinski *et al.* [81] recently extended the idea of using fractionally charged pseudo-atoms to modify the total charge of the water molecules in an aqueous electrolyte, although at the price of relinquishing control over the distribution of charges within the electrolyte.

We emphasize that modelling the computational counter electrode either as a charged continuum region outside the explicit electrolyte or as an object

Charging the supercell		Application to solid/liquid interfaces			
Method	Charging	Geometry		Boundary conditions	Electrode potential
		slab	solv		
MTP ^a [65], [68]	continuous	sym	vac	const $E \oplus D^b$	no
DC ^c [57] & GDC ^d [82]	continuous	sym	vac	const E	yes
Sheet charge/jellium [59]	discrete	sym	vac	const D	yes
• DRM ^e [51, 52], [83]			expl impl		yes yes
Electrolyte with net charge					
• VASPsol [76]	continuous	sym	impl	const D	yes
• Environ [77, 84, 85]	continuous	asym	hybrid	const D	yes
• Explicit H ⁺ [70–73]	discrete	asym	expl	const D	yes
• Imbalanced ion conc. [74]	discrete	sym	expl	const D	no
• Fract. charged water [81]	continuous	sym	expl	const D	no
• ESM-RISM ^f [62, 86, 87]	continuous	asym	impl	const E	yes
CIP-DFT ^g [78]	continuous	asym	hybrid	const E	yes
FCP ^h [48] [88]	continuous	asym	expl	const $\langle E \rangle$	yes
CCE ⁱ [79], [49], [47]	continuous	asym	expl	const $\langle E \rangle$	yes
FSE ^j [89]	continuous	asym	expl	const $\langle E \rangle$	yes

^aModern theory of polarization

^b \oplus : Exclusive or

^cDipole correction

^dGeneralized dipole correction

^eDouble-reference method

^fEffective screening medium - Reference interaction site model

^gConstant inner potential DFT

^hFictitious charge particle method

ⁱComputational counter electrode

^jFully solvated electrode

Table 1 Methods to charge supercells and model electrochemical solid/liquid interfaces, and their key properties/approximations.

consisting of actual atoms creates a hydrophobic gap between the computational counter electrode and the electrolyte, leading to an undesired and non-negligible potential drop within this region [47]. Moreover, this interfacial potential loss at the computational counter electrode increases the likelihood of reaching a dielectric breakthrough [90] as the field strength increases (see also discussion in section 4).

To eliminate the hydrophobic gap at the computational counter electrode and any associated potential loss, in a newer development [89] the setup proposed by Surendralal *et al.* [79] has been extended to the use of a fully solvated electrode, cf. Fig. 4f. In this approach a Gaussian counter charge, placed within the aqueous region, is used to charge the working electrode. While this method requires slight modifications in the DFT code, it enables considerably larger potential drops and realistically strong electric fields at the working electrode/water interface. Moreover, future developments will enable an accurate description of the diffuse region at the interface by exchanging the Gaussian charge for a selfconsistently determined counter charge distribution, that accurately describes the charge density distribution of the double layer in that region.

4 Band structure perspective on electrochemical interfaces

While it is straightforward to apply electric fields in empirical molecular dynamics [49], special care must be taken in the context of electronic structure simulations. Fig. 5a shows a schematic representation of a prototypical interface under electric bias between a metal working electrode, explicit electrolyte (H₂O) and a computational counter electrode. The counter electrode can be realized as discussed in the preceding section.

In this setup, the electrolyte band gap defines the maximum possible potential drop, that can be applied across the electrolyte: if the applied voltage U equals the band gap E_g , the energetic position of the conduction band minimum (CBM) at one side becomes equal to the energetic position of the valence band maximum (VBM) at the other side due to band bending. Fig. 5a depicts a situation where the applied voltage U is only slightly less than E_g . For $U > E_g$ dielectric breakthrough sets in. Therefore, the maximum electric field that can be achieved is $\|\vec{E}_{max}\| = E_g/d$, where d is the thickness of the electrolyte.

We emphasize that in practical calculations, however, the maximum electric field is often much smaller than E_g/d : it also depends on the alignment of the Fermi level E_F of the working electrode with respect to the band edges of the electrolyte at zero electrode charge (potential of zero charge: PZC). Although E_F can be freely adjusted within E_g , dielectric breakthrough equally occurs if the Fermi level coincides with either the VBM or CBM, respectively, at any location within the simulation cell due to the tilted bands. Such a situation is shown schematically in Fig. 5b: at the PZC, the Fermi level is located in close vicinity to the VBM. Transferring a charge q from the working electrode to the computational electrode - which is possible for the electronic structure shown in Fig. 5a - now lifts the VBM at the right hand side above E_F , causing dielectric breakthrough. The charge Δq contained in those valence states that are lifted above E_F flows back into the working electrode, so that the VBM becomes equal to E_F : as a consequence, the Fermi level is pinned. The maximum critical field \vec{E}_{max} that can be applied is, hence, the one just before Fermi level pinning occurs.

In the present setup, the maximum electric field that can be applied depends on the thickness of the water slab contained within the simulation cell. At constant applied voltage, the total electric field decreases with increasing distance between the working and computational counter electrodes. For desirable cell sizes, these fields often fall short of realistic interfacial electric field strengths. The reason is that nature deposits the counter charges in the form of ions much closer to the electrode surface than possible via the computational counter electrodes depicted in Figs. 5a,b. Ref. [89] therefore suggested to decouple the position of the computational counter electrode from the edge of the explicit electrolyte region and place the counter charge directly within the electrolyte, cf. Fig. 5c. This allows achieving much stronger electric fields at the same applied voltage without causing dielectric breakthrough.

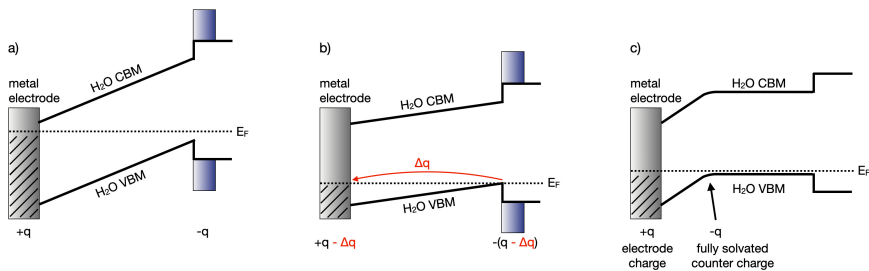


Fig. 5 **a)** Schematic representation of the band structure across an electrode-electrolyte interface. The field is applied via a semiconducting computational counter electrode (CCE) outside the electrolyte region. The Fermi level can be adjusted freely within the electronic gap of the electrolyte and the CCE. **b)** Sufficiently strong applied fields are able to tilt the bands of the electrolyte, so that the Fermi level straddles either the valence or conduction band edge. Dielectric breakthrough will occur. A corresponding charge transfer between the working electrode and the CCE reduces the field so that the Fermi level is moved back to the band edge. **c)** Stronger fields can be applied at the same voltage without dielectric breakthrough by moving the counter charge closer to the working electrode surface.

Here we emphasize that the situation is further complicated by the fact, that the applied electric field $\vec{E} = \varepsilon_0^{-1}[\vec{D} - \vec{P}]$ consists of two components: the equal and opposite charges q on the working electrode and the computational counter electrode give rise to an electric displacement \vec{D} . In response to the electric displacement, the electrolyte becomes polarized with an ensuing polarization density \vec{P} . It is, however, their sum - the total field \vec{E} - which is responsible for the band bending illustrated in Fig. 5. Accordingly, one may choose to work within different electrostatic boundary conditions of $\vec{D} = \text{const.}$ or $\vec{E} = \text{const.}$, as outlined in section 2.

As a consequence, it may be tempting to use $\vec{D} = \text{const.}$ and directly put the targeted charge on the working electrode. Unfortunately, the electrolyte is unable to reorganize instantaneously. For strongly polar solvents like water, in equilibrium \vec{D} and \vec{P} cancel out on average to a large degree, due to the large dielectric constant of water. The polarization density in the electrolyte is formed due to molecular reorientation and ion diffusion. These proceed on rather long time scales compared to those accessible in electronic structure simulations. Hence, polarizing a metal-electrolyte interface usually requires several tens of picoseconds [47]. Directly charging the working electrode under $\vec{D} = \text{const.}$ to its target value, without giving the electrolyte sufficient time to polarize, immediately causes dielectric breakthrough, preventing in most cases even convergence of the DFT self-consistency loop.

One may argue that the $\vec{D} = \text{const.}$ approach may be applied safely by increasing the electrode charge q only in sufficiently small increments, cf., e.g., Ref. [79]. This is true in principle. However, as discussed above, the electrons and ions undergo thermal fluctuations. By extension, their thermal movement creates fluctuations in the polarization density $\vec{P}(t)$, which lead to potential fluctuations on the order of $\sqrt{k_B T/C} \sim 1$ eV. Even if q is changed in only small

Any such control scheme relies on a conjugate pair of extensive and intensive quantities - such as entropy and temperature (thermostat), or volume and pressure (barostat) - where the extensive quantity is used to drive the fluctuating intensive one to a desired target value¹. In the context of potential control, it is straightforwardly shown that the electrode charge n and the electrode potential Φ , form such a pair of conjugate quantities [49]. Since the electrode is connected to an external reservoir of charge, constructing a potentiostat amounts to deriving an equation of motion for the extensive charge $n_e(t)$, i. e. the exchange of charge between the electrode at potential $\Phi(t)$ and the external reservoir held at Φ_0 .

This task is complicated by the fact that the potentiostat is intended to describe the exchange of charge with a reservoir not just in static calculations, but in the context of molecular dynamics at finite temperature. The thermal motion of the electrons and ions, as well as the exchange of charge between the electrode and the reservoir, create thermal fluctuations in the electric field and - by extension - in the system potential $\Phi(t)$. In the physical system, the identical argument applies to the external environment directly adjacent to the microscopic region targeted by our simulations. Therefore, our supercell is embedded in the fluctuating electric field created by the thermal motion of the electrons and ions in its local external environment.

It is the role of the potentiostat to mimic the contact of the supercell with this external environment, cf. Fig. 6. If the reservoir of charge were to be held at an exactly constant potential without any thermal fluctuations (corresponding to $T = 0$ K), the supercell would be able to dissipate its thermal potential fluctuations into the external reservoir, thereby violating the 2nd law of thermodynamics. Such an artificial net energy drain would constantly drive the simulation system out of equilibrium. In order to prevent such a spurious energy transfer, the electric field fluctuations generated along the MD trajectory must be in thermodynamic equilibrium with the field fluctuations of the external environment at the boundary of the supercell. Therefore, the external reservoir itself must have a finite temperature.

The first such approach was introduced in 2012 by Bonnet *et al.* [48], who drove the exchange of charge between electrode and reservoir via a Nose-Hoover algorithm. The Nose-Hoover approach is known to perform well for reasonably ergodic degrees of freedom. The electrode charge, however, is only a single degree of freedom and thus requires Nose-Hoover chains at the cost of an increased number of parameters (Nose-masses) and associated extra tuning. Moreover, the absence of suitable computational counter electrodes in 2012 led Bonnet *et al.* to construct their potentiostat for systems carrying a net excess charge. Hence, the Nose-Hoover potentiostat requires the derivative of the total energy with respect to the net excess charge as an input quantity.

¹We note that in the case of thermostats, the entropy is difficult to control in simulations. There is a need, hence, to perform a Legendre transformation in order to control the temperature via the particle kinetic energies instead. For barostats, in contrast, the volume is straightforwardly adjusted. In that respect, the construction of a potentiostat is conceptually much closer to a barostat than to a thermostat.

This quantity is notoriously difficult to obtain in DFT simulations. Those requirements proved to be serious obstacles in implementing the Nose-Hoover potentiostat into existing DFT codes.

A general approach toward control schemes is provided by the fluctuation-dissipation theorem [26]: Due to the exchange of particles or energy with the reservoir, the system is able to perform external work and dissipate energy. At the same time, the thermal fluctuations of the external environment return energy to the system. In thermodynamic equilibrium, the dissipation and the energy gain from the fluctuations are exactly equal, on average.

In the context of potential control, driving the system potential $\Phi(t)$ towards the external potential Φ_0 is the dissipation. Formally, in an equivalent circuit approach, the dissipation can be represented as a resistance R between the part of the working electrode located inside the supercell and its surrounding external environment, cf. Fig. 6. Physically, R describes the surface conductivity of the electrode surface. This dissipation must then be balanced by the energy gained from the thermal potential fluctuations of the local external environment at the boundary of the supercell. In the equivalent circuit approach, the fluctuations are then given by the Johnson-Nyquist noise generated by the resistance R . It was shown in Ref. [49], that the fluctuation-dissipation theorem in this case takes the form

$$f dt = \underbrace{-\frac{1}{\tau_\Phi}(\Phi - \Phi_0) dt}_{\text{dissipation}} + \underbrace{\sqrt{\frac{2}{\tau_\Phi} \frac{k_B T}{C_0}} dW_t}_{\text{fluctuation}},$$

where f is the rate of change of the electrode potential Φ , τ_Φ is a relaxation time constant and dW_t is the time differential of the Wiener stochastic process.

We emphasize that this energy balance amounts to zero, on average, only in thermodynamic equilibrium, i. e. if the temperatures of the external environment and the supercell are equal. If, e. g., the temperature of the supercell is above the one of the external environment, the dissipation dominates. On the other hand, if the temperature of the supercell is less than the one of the environment, the energy gain via the fluctuations exceeds the dissipation. Therefore, any viable approach to potential control invariably acts also as a thermostat.

Such a *thermopotentiostat* was recently derived by Deißbeck *et al.* [47, 49] via Ito integration [91] of the fluctuation-dissipation relation shown above. Thereby, the thermopotentiostat provides a direct expression for the charge n_{e^-} at each discrete MD time step, under the open thermodynamic boundary conditions depicted in Fig. 6. In contrast to the $D = \text{const.}$ and $E = \text{const.}$ approaches, no artificial constraints on either the charge or potential dynamics are imposed². Instead, the thermopotentiostat is mathematically guaranteed to sample the charge and potential distributions depicted in Fig. 2c, which

²In the limit of setting the equivalent resistance R (or by extension the relaxation time τ_Φ) to either zero or infinity, respectively, electrostatic boundary conditions of $\vec{E} = \text{const.}$ or $\vec{D} = \text{const.}$ are recovered.

preserve the reactive area under charge transfer reactions. In addition, it no longer requires the derivative of the total energy with respect to the charge as an input quantity. Instead, $\Phi(t) - \Phi_0$ is the only mandatory input quantity. In computational setups such as the ones shown in Figs. 4b, c, e, f this potential difference can be conveniently measured via the total dipole moment - given, e. g., by the dipole correction [58] - along the normal direction of the electrode surface. Therefore, in conjunction with any of those computational setups the thermopotentiostat can be straightforwardly included in any electronic structure package.

6 Conclusion

Electrochemical interfaces are thermodynamically open systems, that exchange energy, electronic charge as well as ions with their environment. In addition, on the length and time scale relevant for chemical reactions large spatial and temporal fluctuations of the electrostatic potential and field occur. Including these features in realistic *ab initio* simulations is challenging.

In this review, we have systematically analyzed the fundamental nature and the physics behind these challenges. They are related to three main issues: First, electrostatic phenomena arising from the long-range nature of the Coulomb interaction in small supercells with periodic boundary conditions. Issues discussed here relate to the choice and arrangement of the computational counter electrode. A second main point addressed the phenomena and corrections necessary to describe these interfaces on the small length scale characteristic to DFT supercells. An important point here are the charge and field fluctuations and how they can be consistently included by a careful choice of boundary conditions. The corresponding stochastic potentiostat features the same ease of application as the more commonly used thermostats. Finally, we discussed issues related to band structure and band alignment, which need to be addressed to avoid unphysical simulation artifacts, e.g. by a dielectric breakthrough or to understand limitations in the achievable maximum fields or applied voltages.

Based on this analysis we discussed the available techniques and simulation approaches to address and overcome these limitations. While these methodological developments provide researchers with a new level of realism to study fundamental electrochemical mechanisms and reactions using *ab initio* techniques, critical aspects remain open.

On one side, these simulations are computationally extremely expensive, limiting fully *ab initio* MD simulations with explicit water and electric fields to a few dozen picoseconds. This often limits our ability to get thermodynamically well-converged properties, explore rare events such as chemical reactions with high barriers, or to use improved DFT exchange-correlation functionals, e.g. hybrid functionals, which could help to overcome issues related to the severely underestimated bandgap of water when using semi-local functionals such as GGA. The recent success of machine learning potentials shows great potential

to substantially speed up such calculations. However, in contrast to many of the existing approaches where short-range potentials with an interaction cut-off radius of a few Angstrom are sufficient, the inherent electrostatic nature of electrochemical interfaces makes the inclusion of the long-range Coulomb interactions mandatory. Alternatively, improved implicit solvation or micro-solvation techniques that include a limited amount of explicit solvent directly at the electrified interface are conceivable. Also hybrid approaches, where machine learning is used to describe the dielectric response of the electrolyte to the electrified interface may be promising to reach realistic time scales. Moreover, the computational demand can be reduced even further by advanced sampling techniques, such as, e.g., umbrella sampling or metadynamics [92], upsampling [93], as well as accelerated molecular dynamics approaches, such as forward flux sampling [94, 95].

On another note, implementing grand-canonical boundary conditions not only with respect to the electrode charge, but also in chemical space has remained very challenging in the context of *ab initio* molecular dynamics simulations. Achieving pH-control, in particular, will be needed. A possible route could be via hybrid QM/MM approaches, where hydronium ions are exchanged grand-canonically between the *ab initio* simulation cell and the region modelled via, e.g., machine learning potentials or microsolvation.

Realizing these emerging techniques will provide access to more realistic time and length scales, as well as thermodynamically well-converged properties such as, e.g., reaction rates. Many electrochemical or -catalytical interfaces exhibit a multitude of possible reactions – some desired, some detrimental – with highly complex reaction networks. In turn, the developments outlined above will enable the exploration of these reaction networks and their critical mechanisms at first principles accuracy. The concepts and algorithms discussed in this review should be straightforwardly applicable to these extensions, opening a computationally efficient and physically consistent approach to address many of the still open issues related to electrochemical systems and reactions.

References

- [1] Wang, Y., Song, Y., Xia, Y.: Electrochemical capacitors: mechanism, materials, systems, characterization and applications. *CHEMICAL SOCIETY REVIEWS* **45**(21), 5925–5950 (2016). <https://doi.org/10.1039/c5cs00580a>
- [2] Wang, G., Zhang, L., Zhang, J.: A review of electrode materials for electrochemical supercapacitors. *Chemical Society Reviews* **41**(2), 797–828 (2012). <https://doi.org/10.1039/c1cs15060j>
- [3] Zhu, Y., Murali, S., Stoller, M.D., Ganesh, K.J., Cai, W., Ferreira, P.J., Pirkle, A., Wallace, R.M., Cychosz, K.A., Thommes, M., Su, D., Stach, E.A., Ruoff, R.S.: Carbon-based supercapacitors produced by activation of graphene. *Science* **332**(6037), 1537–1541 (2011). <https://doi.org/10.1126/science.1200770>
- [4] Simon, P., Gogotsi, Y.: Materials for electrochemical capacitors, pp. 320–329. https://doi.org/10.1142/9789814287005_0033. https://www.worldscientific.com/doi/abs/10.1142/9789814287005_0033
- [5] Koetz, R., Carlen, M.: Principles and applications of electrochemical capacitors. *Electrochimica Acta* **45**(15), 2483–2498 (2000). [https://doi.org/10.1016/S0013-4686\(00\)00354-6](https://doi.org/10.1016/S0013-4686(00)00354-6)
- [6] Lee, J.-S., Kim, S.T., Cao, R., Choi, N.-S., Liu, M., Lee, K.T., Cho, J.: Metal-air batteries with high energy density: Li-air versus zn-air. *Advanced Energy Materials* **1**(1), 34–50 (2011). <https://doi.org/10.1002/aenm.201000010>
- [7] Suntivich, J., Gasteiger, H.A., Yabuuchi, N., Nakanishi, H., Goodenough, J.B., Shao-Horn, Y.: Design principles for oxygen-reduction activity on perovskite oxide catalysts for fuel cells and metal-air batteries. *Nature Chemistry* **3**(7), 546–550 (2011). <https://doi.org/10.1038/nchem.1069>
- [8] Cheng, F., Chen, J.: Metal-air batteries: from oxygen reduction electrochemistry to cathode catalysts. *Chemical Society Reviews* **41**(6), 2172–2192 (2012). <https://doi.org/10.1039/c1cs15228a>
- [9] Wang, Z.-L., Xu, D., Xu, J.-J., Zhang, X.-B.: Oxygen electrocatalysts in metal-air batteries: from aqueous to nonaqueous electrolytes. *Chemical Society Reviews* **43**(22), 7746–7786 (2014). <https://doi.org/10.1039/c3cs60248f>
- [10] Li, Y., Lu, J.: Metal air batteries: Will they be the future electrochemical energy storage device of choice? *ACS Energy Letters* **2**(6), 1370–1377 (2017). <https://doi.org/10.1021/acsenerylett.7b00119>

- [11] Hwang, S.-W., Tao, H., Kim, D.-H., Cheng, H., Song, J.-K., Rill, E., Brenckle, M.A., Panilaitis, B., Won, S.M., Kim, Y.-S., Song, Y.M., Yu, K.J., Ameen, A., Li, R., Su, Y., Yang, M., Kaplan, D.L., Zakin, M.R., Slepian, M.J., Huang, Y., Omenetto, F.G., Rogers, J.A.: A physically transient form of silicon electronics. *Science* **337**(6102), 1640–1644 (2012). <https://doi.org/10.1126/science.1226325>
- [12] Yu, K.J., Kuzum, D., Hwang, S.-W., Kim, B.H., Juul, H., Kim, N.H., Won, S.M., Chiang, K., Trumpis, M., Richardson, A.G., Cheng, H., Fang, H., Thompson, M., Bink, H., Talos, D., Seo, K.J., Lee, H.N., Kang, S.-K., Kim, J.-H., Lee, J.Y., Huang, Y., Jensen, F.E., Dichter, M.A., Lucas, T.H., Viventi, J., Litt, B., Rogers, J.A.: Bioresorbable silicon electronics for transient spatiotemporal mapping of electrical activity from the cerebral cortex. *Nature Materials* **15**(7), 782 (2016). <https://doi.org/10.1038/NMAT4624>
- [13] Ledesma, H.A., Tian, B.: Nanoscale silicon for subcellular biointerfaces. *Journal of Materials Chemistry B* **5**(23), 4276–4289 (2017). <https://doi.org/10.1039/c7tb00151g>
- [14] Tian, B., Xu, S., Rogers, J.A., Cestellos-Blanco, S., Yang, P., Carvalho-de-Souza, J.L., Bezanilla, F., Liu, J., Bao, Z., Hjort, M., Cao, Y., Melosh, N., Lanzani, G., Benfenati, F., Galli, G., Gygi, F., Kautz, R., Gorodetsky, A.A., Kim, S.S., Lu, T.K., Anikeeva, P., Cifra, M., Krivosudsky, O., Havelka, D., Jiang, Y.: Roadmap on semiconductor-cell biointerfaces. *PHYSICAL BIOLOGY* **15**(3) (2018). <https://doi.org/10.1088/1478-3975/aa9f34>
- [15] Sabat, K.C., Rajput, P., Paramguru, R.K., Bhoi, B., Mishra, B.K.: Reduction of oxide minerals by hydrogen plasma: An overview. *Plasma Chemistry and Plasma Processing* **34**(1), 1–23 (2014). <https://doi.org/10.1007/s11090-013-9484-2>
- [16] Cavaliere, P.: Hydrogen Assisted Direct Reduction of Iron Oxides. Springer, ??? (2022). <https://doi.org/10.1007/978-3-030-98056-6>
- [17] Lin, H.Y., Chen, Y.W., Li, C.P.: The mechanism of reduction of iron oxide by hydrogen. *Thermochimica Acta* **400**(1-2), 61–67 (2003). [https://doi.org/10.1016/S0040-6031\(02\)00478-1](https://doi.org/10.1016/S0040-6031(02)00478-1)
- [18] Spreitzer, D., Schenk, J.: Reduction of iron oxides with hydrogen - a review. *Steel Research International* **90**(10) (2019). <https://doi.org/10.1002/srin.201900108>
- [19] Magnussen, O.M., Groß, A.: Toward an atomic-scale understanding of electrochemical interface structure and dynamics. *Journal of the American Chemical Society* **141**(12), 4777–4790 (2019)

<https://doi.org/10.1021/jacs.8b13188>. <https://doi.org/10.1021/jacs.8b13188>. PMID: 30768905

- [20] Nose, S.: A molecular dynamics method for simulations in the canonical ensemble. *Molec. Phys.* **52**, 255 (1984). <https://doi.org/10.1080/00268978400101201>
- [21] Nose, S.: A unified formulation of the constant temperature molecular dynamics methods. *J. Chem. Phys.* **81**, 511 (1984). <https://doi.org/10.1063/1.447334>
- [22] Berendsen, H.J.C., Postma, J.P.M., van Gunsteren, W.F., DiNola, A., Haak, J.R.: Molecular dynamics with coupling to an external bath. *J. Chem. Phys.* **81**, 3684 (1984). <https://doi.org/10.1063/1.448118>
- [23] Martyna, G.J., Klein, M., Tuckerman, M.: Nosé–hoover chains: The canonical ensemble via continuous dynamics. *J. Chem. Phys.* **97**, 2635 (1992). <https://doi.org/10.1063/1.463940>
- [24] Bussi, G., Donadio, D., Parinello, M.: Canonical sampling through velocity rescaling. *J. Chem. Phys.* **126**, 014101 (2007). <https://doi.org/10.1063/1.2408420>
- [25] Bussi, G., Parinello, M.: Stochastic thermostats: comparison of local and global schemes. *Comput. Phys. Comm.* **179**, 26–29 (2008). <https://doi.org/10.1016/j.cpc.2008.01.006>
- [26] Callen, H.B., Welton, T.A.: Irreversibility and generalized noise. *Phys. Rev.* **83**, 34 (1951). <https://doi.org/10.1103/PhysRev.83.34>
- [27] Ringe, S., Hörmann, N., Oberhofer, H., Reuter, K.: Implicit solvation methods for catalysis at electrified interfaces. *Chem. Rev.* (2021). <https://doi.org/10.1021/acs.chemrev.1c00675>
- [28] Groß, A., Sakong, S.: Modelling the electric double layer at electrode/electrolyte interfaces. *Curr. Op. Electrochem.* **14**, 1–6 (2019). <https://doi.org/10.1016/j.coelec.2018.09.005>
- [29] Huang, L.-F., Scully, J.R., Rondinelli, J.M.: Modeling corrosion with first-principles electrochemical phase diagrams. *Ann. Rev. Mater. Res.* **49**(1), 53–77 (2019). <https://doi.org/10.1146/annurev-matsci-070218-010105>
- [30] Calle-Vallejo, F., Koper, M.T.M.: First-principles computational electrochemistry: Achievements and challenges. *Electrochim. Acta* **84**, 3–11 (2012). <https://doi.org/10.1016/j.electacta.2012.04.062>
- [31] Alfonso, D.R., Tafen, D.N., Kauffmann, D.R.: First-principles modeling

- in heterogeneous electrocatalysis. *Catalysts* **8**(10), 424 (2018). <https://doi.org/10.3390/catal8100424>
- [32] Pastor, E., Lian, Z., Xia, L., Ecija, D., Galán-Mascarós, J.R., Barja, S., Giménez, S., Arbiol, J., López, N., García de Arquer, F.P.: Complementary probes for the electrochemical interface. *Nature Reviews Chemistry* (2024). <https://doi.org/10.1038/s41570-024-00575-5>
- [33] Butler, K.T., Gautam, G.S., Canepa, P.: Designing interfaces in energy materials applications with first-principles calculations. *npj Computational Materials* **5**, 19 (2019). <https://doi.org/10.1038/s41524-019-0160-9>
- [34] Gonella, G., Backus, E.H.G., Nagata, Y., Bonthuis, D.J., Loche, P., Schlaich, A., Netz, R.R., Kühnle, A., McCrum, I.T., Koper, M.T., Wolf, M., Winter, B., Meijer, G., Campen, R.K., Bonn, M.: Water at charged interfaces. *Nature Reviews Chemistry* **5**, 466 (2021). <https://doi.org/10.1038/s41570-021-00293-2>
- [35] Maurice, V., Klein, L.H., Strehblow, H.-H., Marcus, P.: In situ stm study of the surface structure, dissolution, and early stages of electrochemical oxidation of the ag(111) electrode. *J. Phys. Chem. C* **111**, 16351–16361 (2007). <https://doi.org/10.1021/jp0742517>
- [36] Huang, J., Song, G.-L., Atrens, A., Dargusch, M.: What activates the mg surface? a comparison of mg dissolution mechanisms. *Journal of Materials Science and Technology* **57**, 204–220 (2020). <https://doi.org/10.1016/j.jmst.2020.03.060>
- [37] Yuwono, J.A., Birbilis, N., Taylor, C.D., Williams, K.S., Samin, A.J., Medhekar, N.V.: Aqueous electrochemistry of the magnesium surface: Thermodynamic and kinetic profiles. *Corr. Sci.* **147**, 53–68 (2020). <https://doi.org/10.1016/j.corsci.2018.10.014>
- [38] Rossmeis, J., Skulason, E., Björketun, M.E., Tripkovic, V., Norskov, J.K.: Modeling the electrified solid–liquid interface. *Chem. Phys. Lett.* **466**, 68 (2008). <https://doi.org/10.1016/j.cplett.2008.10.024>
- [39] Janik, M.J., Taylor, C.D., Neurock, M.: First-principles analysis of the initial electroreduction steps of oxygen over pt(111). *J. Electrochem. Soc.* **156**(1), 126–135 (2008). <https://doi.org/10.1149/1.3008005>
- [40] Kronberg, R., Laasonen, K.: Coupling surface coverage and electrostatic effects on the interfacial adlayer–water structure of hydrogenated single-crystal platinum electrodes. *The Journal of Physical Chemistry C* **124**(25), 13706–13714 (2020). <https://doi.org/10.1021/acs.jpcc.0c02323>

- [41] Santos, E., Schmickler, W.: Models of electron transfer at different electrode materials. *Chem. Rev.* **122**, 10581–10598 (2022). <https://doi.org/10.1021/acs.chemrev.1c00583>
- [42] Surendralal, S.: Development of an ab initio computational potentiostat and its application to the study of Mg corrosion. PhD thesis, Ruhr-Universität Bochum (2020). <https://hss-opus.ub.ruhr-uni-bochum.de/opus4/frontdoor/index/index/year/2020/docId/7010>
- [43] Omranpoor, A.H., Kox, T., Spohr, E., Kenmoe, S.: Influence of temperature, surface composition and electrochemical environment on 2-propanol decomposition at the $\text{Co}_3\text{O}_4(001)/\text{H}_2\text{O}$ interface. *Applied Surface Science Advances* **12**, 100319 (2022). <https://doi.org/10.1016/j.apsadv.2022.100319>
- [44] Surendralal, S., Todorova, M., Neugebauer, J.: Impact of water coadsorption on the electrode potential of H-Pt(111)-liquid water interfaces. *Phys. Rev. Lett.* **126**, 166802 (2021). <https://doi.org/10.1103/PhysRevLett.126.166802>
- [45] Le, J., Ianuzzi, M., Cuesta, A., Cheng, J.: Determining potentials of zero charge of metal electrodes versus the standard hydrogen electrode from density-functional-theory-based molecular dynamics. *Phys. Rev. Lett.* **119**, 016801 (2017). <https://doi.org/10.1103/PhysRevLett.119.016801>
- [46] Bussi, G., Donadio, D., Parrinello, M.: Canonical sampling through velocity rescaling. *The Journal of Chemical Physics* **126**(1), 014101 (2007) https://pubs.aip.org/aip/jcp/article-pdf/doi/10.1063/1.2408420/15393604/014101_1.online.pdf. <https://doi.org/10.1063/1.2408420>
- [47] Deußenbeck, F., Wippermann, S.: Dielectric properties of nanoconfined water from ab initio thermopotentiostat molecular dynamics. *J. Chem. Theory Comput.* **19**, 1035–1043 (2023). <https://doi.org/10.1021/acs.jctc.2c00959>
- [48] Bonnet, N., Morishita, T., Sugino, O., Otani, M.: First-principles molecular dynamics at a constant electrode potential. *Phys. Rev. Lett.* **109**, 266101 (2012). <https://doi.org/10.1103/PhysRevLett.109.266101>
- [49] Deußenbeck, F., Freysoldt, C., Todorova, M., Neugebauer, J., Wippermann, S.: Dielectric properties of nanoconfined water: A canonical thermopotentiostat approach. *Phys. Rev. Lett.* **126**, 136803 (2021). <https://doi.org/10.1103/PhysRevLett.126.136803>
- [50] Norskov, J.K., Rossmeisl, J., Lindquist, L., Kitchin, J.R., Bligaard, T., Jonsson, H.: Origin of the overpotential for oxygen reduction at a fuel-cell

- cathode. *J. Phys. Chem. B* **108**, 17886 (2004). <https://doi.org/10.1021/jp047349j>
- [51] Filhol, J.-S., Neurock, M.: Elucidation of the electrochemical activation of water over pd by first principles. *Angew. Chem. Int. Ed.* **45**, 402–406 (2006). <https://doi.org/10.1002/anie.200502540>
- [52] Taylor, C.D., Wasileski, S.A., Filhol, J.-S., Neurock, M.: First principles reaction modeling of the electrochemical interface: Consideration and calculation of a tunable surface potential from atomic and electronic structure. *Phys. Rev. B* **73**, 165402 (2006). <https://doi.org/10.1103/PhysRevB.73.165402>
- [53] Schnur, S., Gross, A.: Challenges in the first-principles description of reactions in electrocatalysis. *Catalysis Today* **165**, 129 (2011). <https://doi.org/10.1016/j.cattod.2010.11.071>
- [54] Sulpizi, M., Gageot, M.-P., Sprik, M.: The silica-water interface: How the silanols determine the surface acidity and modulate the water properties. *Journal of Chemical Theory and Computation* **8**(3), 1037–1047 (2012). <https://doi.org/10.1021/ct2007154>
- [55] Ye, Z., Prominski, A., Tian, B., Galli, G.: Probing the electronic properties of the electrified silicon/water interface by combining simulations and experiments. *Proceedings of the National Academy of Sciences* **118**, 2114929118 (2021). <https://doi.org/10.1073/pnas.2114929118>
- [56] Li, C.-Y., Le, J.-B., Wang, Y.-H., Chen, S., Yang, Z.-L., Li, J.-F., Cheng, J., Yian, Z.-Q.: In situ probing electrified interfacial water structures at atomically flat surfaces. *Nature Materials* **18**, 697 (2019). <https://doi.org/10.1038/s41563-019-0356-x>
- [57] Neugebauer, J., Scheffler, M.: Theory of adsorption and desorption in high electric fields. *Surface science* **287**, 572–576 (1993). [https://doi.org/10.1016/0039-6028\(93\)91030-S](https://doi.org/10.1016/0039-6028(93)91030-S)
- [58] Neugebauer, J., Scheffler, M.: Adsorbate-substrate and adsorbate-adsorbate interactions of Na and K adlayers on Al(111). *Phys. Rev. B* **46**, 16067 (1992). <https://doi.org/10.1103/PhysRevB.46.16067>
- [59] Lozovoi, A.Y., Alavi, A., Kohanoff, J., Lynden-Bell, R.M.: Ab initio simulation of charged slabs at constant chemical potential. *J. Chem. Phys.* **115**, 1661 (2001). <https://doi.org/10.1063/1.1379327>
- [60] Freysoldt, C., Grabowski, B., Hickel, T., Neugebauer, J., Kresse, G., Janotti, A., Van de Walle, C.G.: First-principles calculations for point defects in solids. *Rev. Mod. Phys.* **86**, 253–305 (2014). <https://doi.org/10.1103/>

[RevModPhys.86.253](#)

- [61] Freysoldt, C., Neugebauer, J., Van de Walle, C.G.: Fully ab initio finite-size corrections for charged-defect supercell calculations. *Phys. Rev. Lett.* **102**, 016402 (2009). <https://doi.org/10.1103/PhysRevLett.102.016402>
- [62] Otani, M., Sugino, O.: First-principles calculations of charged surfaces and interfaces: A plane-wave nonrepeated slab approach. *Phys. Rev. B* **73**, 115407 (2006). <https://doi.org/10.1103/PhysRevB.73.115407>
- [63] Hamada, I., Otani, M., Sugino, O., Morikawa, Y.: Green's function method for elimination of the spurious multipole interaction in the surface/interface slab model. *Phys. Rev. B* **80**, 165411 (2009). <https://doi.org/10.1103/PhysRevB.80.165411>
- [64] Hamada, I., Sugino, O., Bonnet, N., Otani, M.: Improved modeling of electrified interfaces using the effective screening medium method. *Phys. Rev. B* **88**, 155427 (2013). <https://doi.org/10.1103/PhysRevB.88.155427>
- [65] Umari, P., Pasquarello, A.: Ab initio molecular dynamics in a finite homogeneous electric field. *Phys. Rev. Lett.* **89**, 157602 (2002). <https://doi.org/PhysRevLett.89.157602>
- [66] Resta, R.: Macroscopic polarization in crystalline dielectrics: the geometric phase approach. *Rev. Mod. Phys.* **66**, 899 (1994). <https://doi.org/10.1103/RevModPhys.66.899>
- [67] Stengel, M., Spaldin, N.A.: Ab initio theory of metal-insulator interfaces in a finite electric field. *Phys. Rev. B* **75**, 205121 (2007). <https://doi.org/10.1103/PhysRevB.75.205121>
- [68] Stengel, M., Spaldin, N.A., Vanderbilt, D.: Electric displacement as the fundamental variable in electronic-structure calculations. *Nature Physics* **5**, 304–308 (2009). <https://doi.org/10.1038/nphys1185>
- [69] Publicly available DFT codes: <https://dft.sandia.gov/quest/dft.codes.html>
- [70] Hansen, M.H., Rossmeisl, J.: Finite bias calculations to model interface dipoles in electrochemical cells at the atomic scale. *J. Phys. Chem. C* **120**, 13485 (2016). <https://doi.org/10.1021/acs.jpcc.6b00721>
- [71] Hansen, M.H., Jin, C., Thygesen, K.S., Rossmeisl, J.: *pH* in grand canonical statistics of an electrochemical interface. *J. Phys. Chem. C* **120**, 29135 (2016). <https://doi.org/10.1021/acs.jpcc.6b09019>
- [72] Sakong, S., Groß, A.: Water structures on a Pt(111) electrode from

- ab initio molecular dynamic simulations for a variety of electrochemical conditions. *Phys. Chem. Chem. Phys.* **22**, 10431–10437 (2020). <https://doi.org/10.1039/C9CP06584A>
- [73] Omranpoor, A.H., Bera, A., Bullert, D., Linke, M., Salamon, S., Webers, S., Wende, H., Hasselbrink, E., Spohr, E., Kenmoe, S.: 2-propanol interacting with $\text{Co}_3\text{O}_4(001)$: A combined vSFS and AIMD study. *The Journal of Chemical Physics* **158**(16), 164703 (2023). https://pubs.aip.org/aip/jcp/article-pdf/doi/10.1063/5.0142707/18185804/164703_1.5.0142707.pdf. <https://doi.org/10.1063/5.0142707>
- [74] Khatib, R., Kumar, A., Sanvito, S., Sulpizi, M., Cucinotta, C.S.: The nanoscale structure of the Pt-water double layer under bias revealed. *Electrochimica Acta* **391** (2021). <https://doi.org/10.1016/j.electacta.2021.138875>
- [75] Mathew, K., Sundararaman, R., Letchworth-Weaver, K., Arias, T.A., Hennig, R.G.: Implicit solvation model for density-functional study of nanocrystal surfaces and reaction pathways. *J. Chem. Phys.* **140**, 084106 (2014). <https://doi.org/10.1063/1.4865107>
- [76] Mathew, K., Kolluru, V.S.C., Mula, S., Steinmann, S.N., Hennig, R.G.: Implicit self-consistent electrolyte model in plane-wave density-functional theory. *J. Chem. Phys.* **151**, 234101 (2019). <https://doi.org/10.1063/1.5132354>
- [77] Goldsmith, Z.K., Calegari Andrade, M.F., Selloni, A.: Effects of applied voltage on water at a gold electrode interface from ab initio molecular dynamics. *Chemical Science* **12**, 5865 (2021). <https://doi.org/10.1039/d1sc00354b>
- [78] Melander, M.M., Wu, T., Weckman, T., Honkala, K.: Constant inner potential DFT for modelling electrochemical systems under constant potential and bias. *npj Computational Materials* **10**(1), 5 (2024). <https://doi.org/10.1038/s41524-023-01184-4>
- [79] Surendralal, S., Todorova, M., Finnis, M.W., Neugebauer, J.: First-principles approach to model electrochemical reactions: Understanding the fundamental mechanisms behind Mg corrosion. *Phys. Rev. Lett.* **120**, 246801 (2018). <https://doi.org/10.1103/PhysRevLett.120.246801>
- [80] Shiraishi, K.: A new slab model approach for electronic structure calculation of polar semiconductor surface. *J. Phys. Soc. Jpn.* **59**, 3455–3458 (1990). <https://doi.org/10.1143/JPSJ.59.3455>
- [81] Dudzinski, A.M., Diesen, E., Heenen, H.H., Bukas, V.J., Reuter, K.: First

- step of the oxygen reduction reaction on Au(111): A computational study of O₂ adsorption at the electrified metal/water interface. *ACS Catal.* **13**, 12084–12081 (2023). <https://doi.org/10.1021/acscatal.3c02129>
- [82] Freysoldt, C., Mishra, A., Ashton, M., Neugebauer, J.: Generalized dipole correction for charged surfaces in the repeated-slab approach. *Phys. Rev. B* **102**, 045403 (2020). <https://doi.org/10.1103/PhysRevB.102.045403>
- [83] Lespes, N., Filho, J.-S.: Using implicit solvent in ab initio electrochemical modeling: Investigating Li⁺/Li electrochemistry at a Li/solvent interface. *J. Chem. Theory Comput.* **11**, 3375–3382 (2015). <https://doi.org/10.1021/acs.jctc.5b00170>
- [84] Andreussi, O., Dabo, I., Marzari, N.: Revised self-consistent continuum solvation in electronic-structure calculations. *The Journal of Chemical Physics* **136**(6), 064102 (2012). <https://doi.org/10.1063/1.3676407>
- [85] Giannozzi, P., Andreussi, O., Brumme, T., Bunau, O., Buongiorno Nardelli, M., Calandra, M., Car, R., Cavazzoni, C., Ceresoli, D., Cococcioni, M., Colonna, N., Carnimeo, I., Dal Corso, A., de Gironcoli, S., Delugas, P., DiStasio, R.A., Ferretti, A., Floris, A., Fratesi, G., Fugallo, G., Gebauer, R., Gerstmann, U., Giustino, F., Gorni, T., Jia, J., Kawamura, M., Ko, H.-Y., Kokalj, A., Küçükbenli, E., Lazzeri, M., Marsili, M., Marzari, N., Mauri, F., Nguyen, N.L., Nguyen, H.-V., Otero-de-la-Roza, A., Paulatto, L., Poncé, S., Rocca, D., Sabatini, R., Santra, B., Schlipf, M., Seitsonen, A.P., Smogunov, A., Timrov, I., Thonhauser, T., Umari, P., Vast, N., Wu, X., Baroni, S.: Advanced capabilities for materials modelling with quantum espresso. *Journal of Physics: Condensed Matter* **29**(46), 465901 (2017). <https://doi.org/10.1088/1361-648X/aa8f79>
- [86] Nishihara, S., Otani, M.: Hybrid solvation models for bulk, interface, and membrane: Reference interaction site methods coupled with density functional theory. *Phys. Rev. B* **96**, 115429 (2017). <https://doi.org/10.1103/PhysRevB.96.115429>
- [87] Hagiwara, S., Nishihara, S., Kuroda, F., Otani, M.: Development of a dielectrically consistent reference interaction site model combined with the density functional theory for electrochemical interface simulations. *Phys. Rev. Materials* **6**, 093802 (2022). <https://doi.org/10.1103/PhysRevMaterials.6.093802>
- [88] Bouzid, A., Pasquarello, A.: Redox levels through constant fermi-level ab initio molecular dynamics. *J. Chem. Theory Comput.* **13**(4), 1769–1777 (2017). <https://doi.org/10.1021/acs.jctc.6b01232>
- [89] Deissenbeck, F., Surendralal, S., Todorova, M., Wippermann, S., Neugebauer, J.: Anomalous hydrogen evolution on magnesium: a fully solvated

electrode approach

- [90] Yoo, S.-H., Todorova, M., Wickramaratne, D., Weston, L., Van de Walle, C.G., Neugebauer, J.: Finite-size correction for slab supercell calculations of materials with spontaneous polarization. *npj Computational Materials* **7**, 58 (2021). <https://doi.org/10.1038/s41524-021-00529-1>
- [91] Gardiner, C.: *Stochastic Methods*. Springer, Berlin (2009)
- [92] Laio, A., Parrinello, M.: Escaping free-energy minima. *Proceedings of the National Academy of Sciences* **99**(20), 12562–12566 (2002) <https://www.pnas.org/doi/pdf/10.1073/pnas.202427399>. <https://doi.org/10.1073/pnas.202427399>
- [93] Jung, J.H., Srinivasan, P., Forslund, A., Grabowski, B.: High-accuracy thermodynamic properties to the melting point from ab initio calculations aided by machine-learning potentials. *npj Computational Materials* **9**(1), 3 (2023). <https://doi.org/10.1038/s41524-022-00956-8>
- [94] Allen, R.J., Frenkel, D., ten Wolde, P.R.: Forward flux sampling-type schemes for simulating rare events: Efficiency analysis. *The Journal of Chemical Physics* **124**(19), 194111 (2006) https://pubs.aip.org/aip/jcp/article-pdf/doi/10.1063/1.2198827/13451756/194111_1_online.pdf. <https://doi.org/10.1063/1.2198827>
- [95] Allen, R.J., Valeriani, C., ten Wolde, P.R.: Forward flux sampling for rare event simulations. *Journal of Physics: Condensed Matter* **21**(46), 463102 (2009). <https://doi.org/10.1088/0953-8984/21/46/463102>